Anti-lock braking control based on bearing load sensing

Kerst, Stijn; Shyrokau, Barys; Holweg, Edward

Publication date
2015

Published in
Proceedings EuroBrake 2015

Citation (APA)
Kerst, S., Shyrokau, B., & Holweg, E. (2015). Anti-lock braking control based on bearing load sensing. In *Proceedings EuroBrake 2015* Article EB2015-ACC-002 FISITA.

EB2015-ACC-002

ANTI-LOCK BRAKING CONTROL BASED ON BEARING LOAD SENSING

[1]Kerst, Stijn[*]; [1]Shyrokau, Barys; [1]Holweg, Edward
[1]Technische Universiteit Delft, The Netherlands

KEYWORDS – Anti-lock Braking, load based control, force based ABS, experimental investigation, load-sensing bearing

ABSTRACT
Research objective: Anti-lock braking algorithms use either/both wheel deceleration and wheel slip to obtain a stable limit cycle around the friction peak to guarantee vehicle steerability and to minimize braking distance. However, both control variables pose several well-known issues regarding ABS control. The usage of wheel loads, for instance estimated based on bearing deformation, could provide a solution to these control variable related difficulties. In this paper, a wheel load based method to control wheel slip is presented and implemented in a novel Anti-lock Braking algorithm. Due to the fundamentally different approach to tackle the issue, numerous well known pitfalls of traditional Anti-lock Braking Systems can be avoided.

Methodology: A mathematical derivation of the quarter car model provides the conditions in which wheel load measurement allows for determination of the derivative of wheel slip. Based on this theory, a novel ABS algorithm is proposed. It consists of two operational phases to control the wheel slip derivative and a phase switching mechanism, all based solely on wheel loads. Furthermore a methodology of wheel load estimation based on bearing deformation measurement is proposed. Finally, an experimental on-road investigation of the load estimation and proposed algorithm is carried out using an instrumented test vehicle.

Results: An on-road investigation with a test vehicle demonstrates the accuracy of wheel load estimation based on bearing deformation. The estimated loads are used in a novel ABS algorithm to demonstrate the feasibility and advantages of load based ABS control.

Limitations of this study: Only straight-line braking is considered as the method of load estimation is currently unable to provide the required bandwidth on estimation of loads when steering.

What does the paper offer that is new in the field: Current research in the field of ABS algorithms is primarily focused on wheel slip and/or wheel deceleration control. The presented study investigates a fundamentally different approach by the use of a novel sensor.

Conclusion: Based on a mathematical derivation a novel load-based ABS algorithm is proposed. Furthermore a methodology of load sensing by the use of instrumented bearings is presented. The performance of both load sensing and the Anti-lock braking algorithm has been checked via experimental testing using an instrumented test vehicle.

I INTRODUCTION

Nowadays the anti-lock braking system is a mandatory active safety system in road vehicles. Its primary function is to prevent wheel lock during heavy braking to guarantee brake performance while simultaneously maintaining vehicle steerability and stability. Although research activities in ABS have been started many years ago, new approaches are continuously being developed and discussed in the automotive research society.

The diversity of the applied control methods in ABS design ranges from bang-bang control up to modern control techniques like model predictive control, iterative learning and others [1, 2]. It should be noted that in literature the investigation of novel ABS control algorithms is often limited by idealistic conditions such as a quarter-car model, homogeneous road friction, simplification of brake system dynamics and other significant assumptions. In industrial realizations, ABS controllers are typically based on a complex set of heuristic rules based on both wheel slip and deceleration. Although this approach dominates in industry, its application requires extra effort to solve well known problems that arise in wheel slip control based on a standard set of vehicle sensors. This includes reference velocity estimation, slip threshold determination and adaptation and functionality at low vehicle speeds.

From a control perspective a force based approach has more potential compared to a kinematic approach. Usage of tire forces allows for the design less complex algorithms whilst maintaining robustness to changing conditions and performance can be enhanced [3]. Estimation techniques or direct/indirect measurement approaches can be used to obtain the control variables. The first approach can be based on a standard set of vehicle sensors; however, it requires a precise system model in real-time causing high computational costs [4]. Methods for direct / indirect wheel force estimation include: tire sidewall or suspension bushing deformation [5], wheel rim strain measurements [6], tire inner liner accelerometer based measurements [7] and a bearing deformation based approach [8]. However, most of these approaches will not offer a high enough bandwidth on the force estimation at the highly nonlinear operation region of ABS.

This paper presents and evaluates a novel wheel load based ABS algorithm as well as a new approach to estimate wheel loading using bearing deformation measurement. The ABS algorithm uses only wheel loads as control variables, in contrast to [3, 9, 10], such to avoid the usage of extra sensors and estimators. Furthermore, whilst other papers use more idealistic laboratory conditions as a tire test rig [3, 9] or a HIL test bench without rotating parts [10], in this paper on-road experiments are carried out. The functionality of the algorithm as well as the quality of wheel load estimation using a bearing deformation based approach is investigated and discussed.

The paper is structured as follows: a general description of a quarter car is presented in Section II. In Section III wheel slip derivative control based on wheel loading is discussed. The novel ABS algorithm is proposed in Section IV. A bearing deformation based method of wheel load reconstruction is discussed in Section V. The experimental setup and test procedures are presented in Section VI. In Section VII experimental results are presented and discussed. Finally, conclusions and future work are discussed in Section VIII.

II QUARTER-CAR DYNAMICS

In section III a mathematical derivation of the quarter-car model will present the conditions which allow for the determination of the wheel slip derivative based on wheel load measurements. In this section the model is presented.

Wheel dynamics, as depicted in Figure 1, can be described by:

$$J\dot{\omega} = r_w F_x - T_b \tag{1}$$

where $\dot{\omega}$ is the angular acceleration of the wheel, F_x is the longitudinal tire force, T_b is the brake torque, J is the moment of inertia of the wheel and r_w is dynamic tire radius. The brake torque is generated through the tangential force at the effective radius of the brake as follows:

$$T_b = r_b F_{TD} \tag{2}$$

where F_{TD} is the tangential force and r_b is the effective friction radius. The tangential force itself is generated by the application of brake pressure to the calliper, this relation is described by:

$$F_{TD} = 2\mu_b P_b A \tag{3}$$

where P_b is the brake pressure at the brake calliper, A is the brake cylinder area and μ_b is the friction coefficient between brake pad and disc. During the braking process the friction coefficient may change due to changes in contact pressure, temperature and velocity.

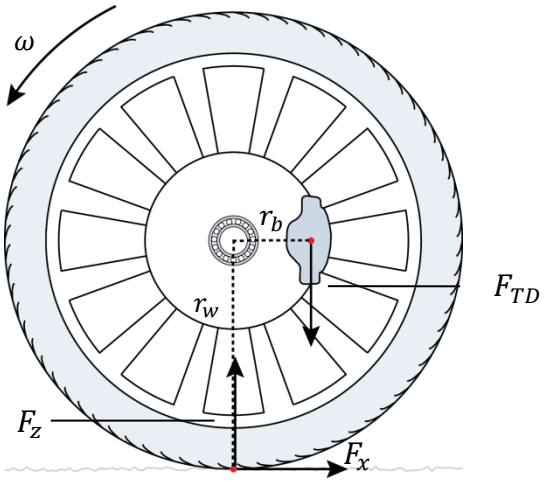

Figure 1: Quarter car model

The longitudinal tire force F_x in Eq. 1 depends on numerous factors including wheel slip, road surface conditions, tire pressure, wheel loading and tire wear. For straight driving this longitudinal force is generally approximated as:

$$F_x = F_z \cdot \mu(\lambda, \vartheta) \tag{4}$$

where F_z is the normal load on the tire and μ is the road-tire friction coefficient. This latter is a non-linear function of wheel slip λ and road surface parameters ϑ. The non-linear friction coefficient function is of significant interest in literature and can be described by piecewise, trigonometric or exponential polynomials [11]. The road surface parameters ϑ characterize the shape of the static tire-road friction curve, whilst the wheel slip determines the actual position on the curve.

During braking, wheel slip λ is defined as:

$$\lambda = \frac{v - r_w \omega}{v} \quad , \quad \lambda \in [0,1] \tag{5}$$

where v represents the vehicle speed and ω is the rotational speed of the wheel.

The longitudinal vehicle dynamics, after neglecting aerodynamic drag, rolling resistance and forces due to road gradients, can be described by:

$$\dot{v} = -\frac{1}{m} \sum_{i=1}^{4} F_{x,i} \tag{6}$$

where m is the vehicle total mass and the sub-indexes i of the longitudinal force indicate the four individual wheels.

III LOAD BASED WHEEL SLIP DERIVATIVE CONTROL

The algorithm proposed in subsection IV is based on control of the wheel slip derivative using wheel load measurements F_x and T_b. The following will present the fundamental backbone on which the algorithm relies. As focus lies on pure load based wheel slip control, wheel and vehicle speeds and accelerations are assumed to be unknown.

First consider the wheel slip derivative, which is obtained by time derivation of Eq. 5:

$$\dot{\lambda} = \frac{r_w \omega}{v^2} \dot{v} - \frac{r_w}{v} \dot{\omega} \tag{7}$$

Note that wheel slip control is represented by control of the left hand side (LHS) of this equation. The right hand side (RHS) of the equation contains unknown vehicle and wheel speeds and accelerations. Now by substituting $\dot{\omega}$ using Eq. 1, $\dot{v}$ using Eq. 6 and multiplying both left and right hand side by v, one obtains

$$v\dot{\lambda} = -\frac{r_w \omega}{v} \frac{1}{m} \sum_{i=1}^{4} F_{x,i} - \frac{r_w}{J} (r_w F_x - T_b) \tag{8}$$

During the situation currently under consideration v is always positive definite, and thus the RHS is indicative for the sign of $\dot{\lambda}$. The RHS can be closely approximated using wheel load measurements F_x and T_b, as will be shown in the following.

The first term in the RHS of Eq. 8, which is the influence of vehicle deceleration on the wheel slip derivative, consists of a vehicle deceleration part, $-\frac{1}{m} \sum_{i=1}^{4} F_{x,i}$, and a vehicle to wheel speed relational term, $\frac{r_w \omega}{v}$. The former term can be closely approximated by the use of the longitudinal force measurements on all wheels and an on-line estimation of the vehicle mass. The wheel speed relational term on the other hand is unknown. However, its bounds can be easily found to be $\in [0,1]$ as the minimum wheel speed is zero, whilst the maximum while braking is limited by the vehicle speed.

The second RHS term in Eq. 8 is governed by the measured loads, wheel inertia J and the dynamic tire radius r_w. In the paper, wheel inertia and dynamic tire radius are assumed to be constant and known.

Note that the complete RHS of Eq. 8 can thus be on-line approximated by load measurements, known boundary values and assumed known parameters. It is therefore possible to define conditions that guarantee a decreasing or increasing wheel slip as follows:

$$IF \quad T_b - r_w F_x < 0 \qquad \Rightarrow \quad \dot{\lambda} < 0 \tag{9}$$

$$IF \quad T_b - r_w F_x > \frac{J}{r_w}\frac{1}{m}\sum_{i=1}^{4} F_{x,i} \qquad \Rightarrow \quad \dot{\lambda} > 0 \tag{10}$$

As the wheel-vehicle speed relation is unknown, a small region remains in which the slip derivative cannot be determined. This is clearly visible in Figure 2(a), where the boundary conditions of Eqs. 9 (dotted line) and 10 (solid line) are presented visually. The $\dot{\lambda}$ region of uncertainty, which can be avoided by a proper control action, can be described by:

$$0 \geq \quad T_b - r_w F_x \quad \leq \frac{J}{r_w}\frac{1}{m}\sum_{i=1}^{4} F_{x,i} \quad \Rightarrow \quad \dot{\lambda} \text{ unknown} \tag{11}$$

Note that as road surface conditions, tire conditions and vertical loading are not within the formulations the methodology is invariant of their states.

IV PROPOSED ANTI-LOCK BRAKING ALGORITHM

The proposed algorithm is a two-phase hybrid controller which ensures a wheel slip limit cycle near the peak of the friction curve. The cyclic behaviour is obtained by the use of two opposing phases; phase 1 ensures a decreasing wheel slip value and phase 2 guarantees an increasing wheel slip. A longitudinal force based mechanism is employed to trigger phase switching. This all results in the cyclic behaviour as depicted in Figure 2(b).

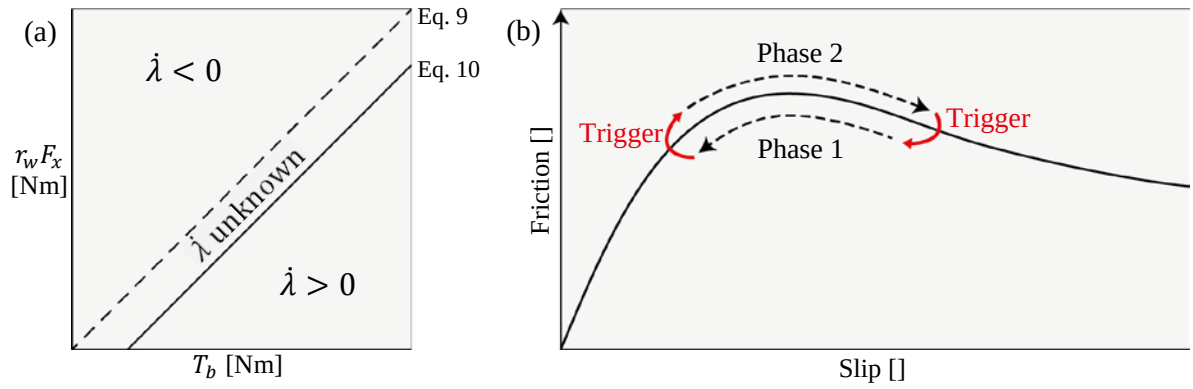

Figure 2: (a) Visualisation of boundary conditions provided by Eqs. 9 and 10 (b) Overview of algorithm

As phase 2 and the triggering mechanism both make use of the maximum longitudinal force encountered within each phase, its definition follows here:

$$\hat{F}_{max}(t) = \max_{t_s \leq \tau \leq t} (F_x(\tau)) \tag{12}$$

where $\hat{F}_{max}$ is the maximum in-phase longitudinal force, t is the current time and t_s is the phase start time. As can be deduced from its definition, the maximum in-phase longitudinal force is reset upon entering a new phase.

Phase 1 – decreasing wheel slip

This phase is initialized when the wheel slip is at the unstable right side of the friction peak, and its goal is to return slip to the stable left side of the friction peak. By doing so, it will increase the road-tire friction. In the proposed algorithm, this is accomplished by ensuring a continuous decrease of wheel slip by setting brake torque T_b based on the state space boundary condition presented in Eq. 9.

As a specific control action is required, it is chosen to offset the boundary condition by an offset parameter. This offset parameter furthermore provides robustness to measurement uncertainties and noise. The following brake torque control law, which ensures a decreasing wheel slip value, is proposed:

$$T_b(\mathrm{t}) = r_w F_x(\mathrm{t}) - \Delta T_b^- \tag{13}$$

where $\Delta T_b^-, \in \langle 0, \infty]$, is the offset parameter. The proposed control law will guarantee a decreasing wheel slip for all road-tire friction conditions.

Phase 2 – increasing wheel slip

After the return to the stable left side of the friction peak in phase 1, this phase aims to increase road-tire friction by increasing wheel slip using the state space boundary conditions for brake torque T_b proposed in Eq. 10.

As in phase 1, an offset parameter is introduced to generate a specific brake torque control action. Besides providing robustness to measurement uncertainties and noise this offset also allows the algorithm to cope with upward changes of the friction peak. Furthermore, in order to optimize the initial brake torque setting, the maximum longitudinal force encountered in the previous phase is used as reference in the initial setting of brake torque. This results in the following control law:

$$T_b(\mathrm{t}) = \frac{J}{r_w}\frac{1}{m}\sum_{i=1}^{4} F_{x,i}(\mathrm{t}) + r_w \cdot \max(\hat{F}_{sp}, \hat{F}_{max}(t)) + \Delta T_b^+ \tag{14}$$

where $\Delta T_b^+, \in \langle 0, \infty]$, is the offset parameter and $\hat{F}_{sp}$ is the longitudinal force set point value. On phase entering the longitudinal force set point value is set such that it contains a scaled value of previous phase's encountered maximum longitudinal force:

$$\hat{F}_{sp} = \alpha_F \hat{F}_{max}(t) \tag{15}$$

where α_F is the longitudinal force scaling parameter which is applied to improve algorithm cycling. The control law is able to cope with changes in friction curve characteristics of both increasing as decreasing friction peak. The decreasing peak is handled as the $\hat{F}_{max}$ setting is reset every phase. The usage of the combination of $\hat{F}_{max}$ and ΔT_b^+ allows for handling of an increasing friction peak, as the brake torque setting is set higher than the estimate of the maximum longitudinal force.

Phase triggering mechanism

When slip boundary conditions of either phase 1 or 2 are satisfied the longitudinal force can be used to determine whether the system is evolving towards or from the friction peak. An increasing longitudinal force represents a movement towards the friction peak while on the other hand a decreasing longitudinal force represents an evolution from the friction peak. The latter should cause a trigger to a subsequent phase.

In order to determine this phase triggering, the maximum in-phase longitudinal force defined in Eq. 12 is used. Whenever the current measured longitudinal force has decreased more than an a priori set amount from the maximum in-phase longitudinal force, the next phase is triggered. This statement can be condensed to the following rule:

$$F_x(t) < \hat{F}_{max}(t) - \Delta F_{tr} \tag{16}$$

where ΔF_{tr} is the a priori determined force offset. This offset is set such that it both minimizes false triggering due to vertical force variations and measurement inaccuracy as

well as friction curve overshoot. The longitudinal force is only indicative of the evaluation of slip with respect to the friction peak when the boundary conditions of Eqs. 9 and 10 are satisfied. The mechanism is therefore only allowed to trigger phases when the system states satisfy these equations.

Note that this triggering mechanism will only work with road surfaces with sufficient friction decrease at the unstable side of the friction peak.

Figure 3 graphically summarizes the proposed control logic.

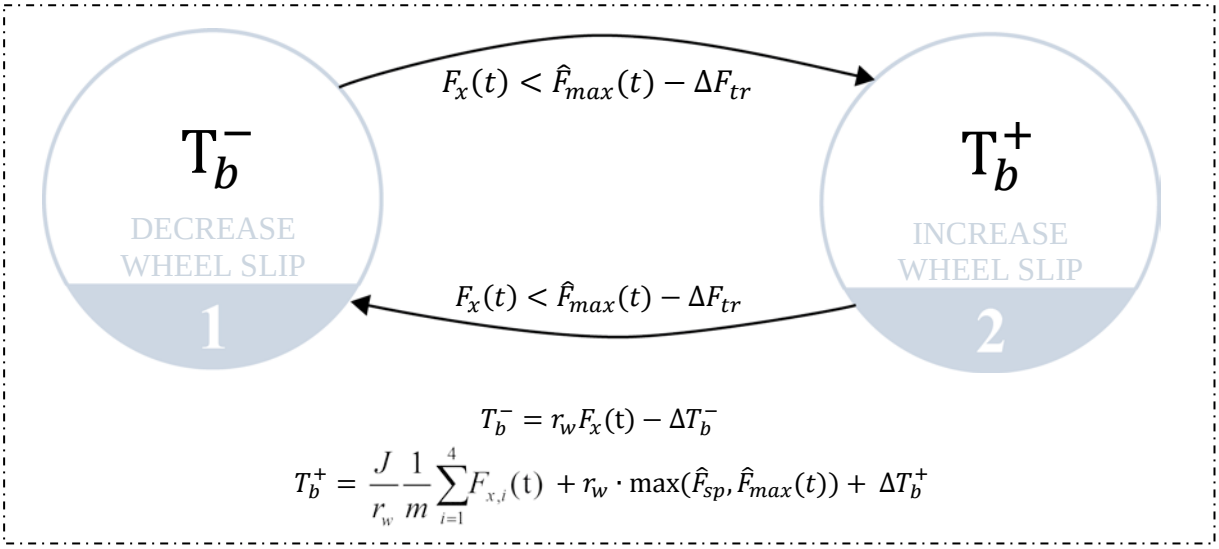

Figure 3: Overview of algorithm logic

Activation and deactivation logic

Activation of the algorithm will take place when similar conditions occur as when the algorithm switches from phase 2 to phase 1. Brake torque should be such that a wheel slip is increasing, while a decrease of longitudinal wheel force is detected.

As the algorithm is still in its development stage, deactivation of the algorithm is not yet considered.

V RECONSTRUCTION OF WHEEL LOADING

In conjunction with industrial partner SKF bearings have been developed on which deformation is measured at several load indicative locations using strain gauges. Based on the measured strains the loads F_x and T_b, necessary for the presented algorithm, can be reconstructed. Note that brake torque T_b acts on the rotary degree of freedom of the bearing and therefore cannot be directly measured. However, the brake torque can be estimated by measurement of the effects of tangential force F_{TD}.

The reconstruction of loads consists of two steps. First all signals are filtered and calibrated such to obtain the unbiased signal contents of interest. Afterwards the loads are determined by transformation of these signals.

Filtering and calibration

In the filtering phase the aim is to filter out oscillations due to the passing of rolling elements. This filtering is performed by a wheel rotational speed dependent notch filter, of which the notch centre frequency f_c is defined as:

$$f_c(t) = \gamma\omega(t) \tag{17}$$

where γ is an a priori empirical determined relation between wheel and rolling element rotational frequencies. The notch bandwidth b_w is set to a value such that minimal disturbance in the signal occurs whilst attenuating the full rolling element disturbance.

Due to temperature gradients within the bearing the deformation signals drift. In order to compensate for this low temperature drift, signals are calibrated upon the start of each experiment. This calibration consists of offsetting all strain measurements to zero. Figure 4 shows an example of the strain measured by one of the strain gauges and its processed version during a braking experiment.

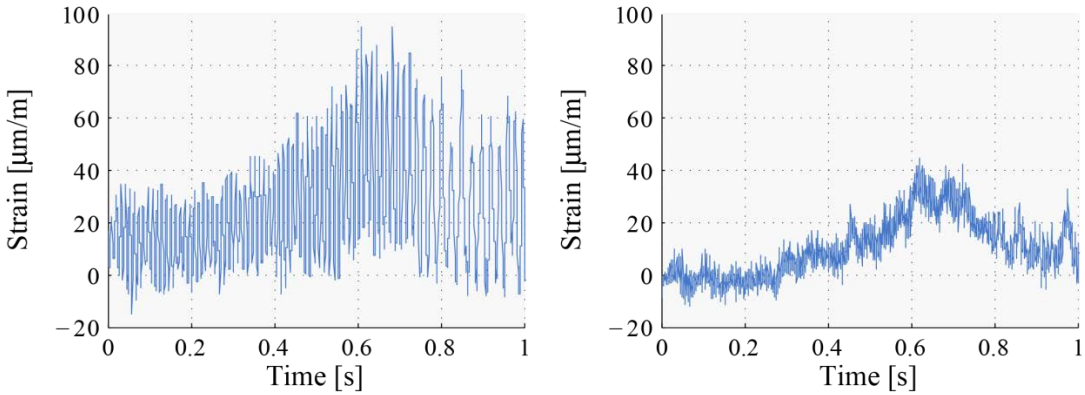

Figure 4: (a) unfiltered strain signal (b) notch filtered and calibrated strain signal

Load reconstruction

By the use of an in-situ calibration, the relation between bearing deformation and wheel load is determined. A linear relation is assumed:

$$\boldsymbol{y} = \boldsymbol{X\beta} + \varepsilon \tag{18}$$

where $\boldsymbol{y}$ is the wheel load vector $(F_x\ T_b)^T$, $\boldsymbol{X}$ is the deformation vector $(x_1 \ldots\ x_n)$ which contains the processed measurements of all n strain gauges, $\boldsymbol{\beta}$ is the parameter vector $(\beta_1 \ldots\ \beta_n)^T$ and ε is the noise term.

The parameter vector $\boldsymbol{\beta}$ is determined using a multivariate normal regression algorithm, which performs a minimization of the sum of the squared residuals. A measurement rim provides the $\boldsymbol{y}$ vector for the determination of this parameter vector.

VI EXPERIMENTAL SETUP

The proposed algorithm is evaluated on a BMW 5-Series test vehicle shown in Figure 5. Vehicle modifications have been performed to accommodate experiments focused on anti-lock braking based on wheel deceleration, wheel slip and wheel loading.

Vehicle modifications

Data acquisition, processing and control determination is performed real-time by the use of a dSPACE AutoBox platform. AD/DA conversion and IO boards provide communications with other installed components, while CAN communication board allows for readout of the vehicle powertrain and chassis CAN busses. Wheel speeds are reconstructed using the encoder block signals tapped at each wheel.

Vehicle braking is controlled through control of the original Bosch DSC 8 hydraulic unit, by dismantling the original DSC unit and installation of a custom coil pack and power electronics. Pressure sensors are installed in the brake lines close to each brake calliper. A feedforward controller, based on a static mapping of the brake system dynamics, allows for brake pressure control at each individual wheel. As the relation between brake pressure and brake torque can be measured using the installed sensors, brake torque can be controlled directly via brake pressure control.

Figure 5: Test vehicle on the Valkenburg airstrip

A VEhicle LOad Sensor (VELOS) measurement wheel is fitted on the front left wheel for determination of benchmark tire forces and moments. Furthermore, both front wheels are equipped with a prototype version of the SKF load-sensing bearing, which is currently in development at the Delft University of Technology.

Test procedure

All test were performed on a single day at an old military air strip during clear weather. The asphalt is a high friction surface resulting in a tire-road friction coefficient with an estimated peak friction at a relatively low level of slip (approximately $\lambda = 0.06$) and a moderate drop-off at the unstable side of the peak. Figure 6 shows the curve fitted Burckhardt friction model based on measured data during the field test.

The test procedure consisted of accelerating the vehicle to the speed of 100 km/h and then applying heavy braking, such to cause ABS activation. Braking was only performed on the front wheels, in order to guarantee lateral stability. Over the course of different tests algorithm parameters $\Delta T_b^-, \Delta T_b^+, \Delta F_{tr}$ and α_{F_x} were tuned in order to improve algorithm performance.

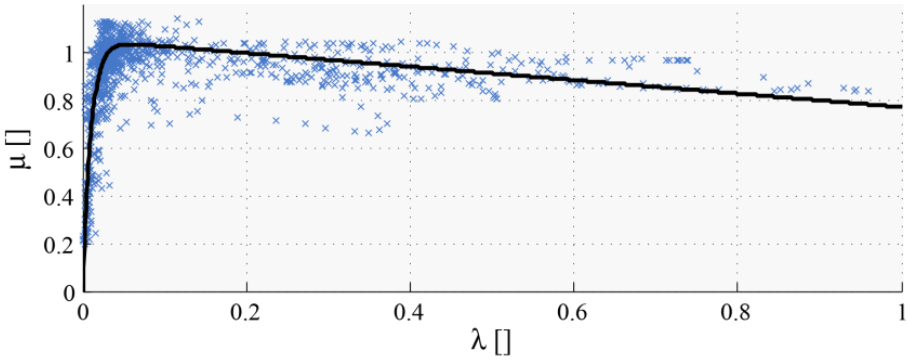

Figure 6: Burckhardt model based fitting of experimental data

Algorithm modifications

As the modified DSC unit only allows for stepwise brake pressure modulation, the continuous control is translated towards discrete pressure steps. At the initiation of each phase the continuous control is sampled at 30ms, such that stepwise brake torque evaluation will result.

VII EXPERIMENTAL RESULTS

Reconstruction of wheel loading

A brief representative capture of both longitudinal force and brake torque in the time domain is shown in Figure 7. Phase 2 of the algorithm is triggered at $t \cong 2.33$ s, which can be clearly seen from the increasing of brake torque and subsequent increase of longitudinal force. It can be noted that both bearing load sensing based measured F_x and T_b are close to the VELOS benchmark measurements.

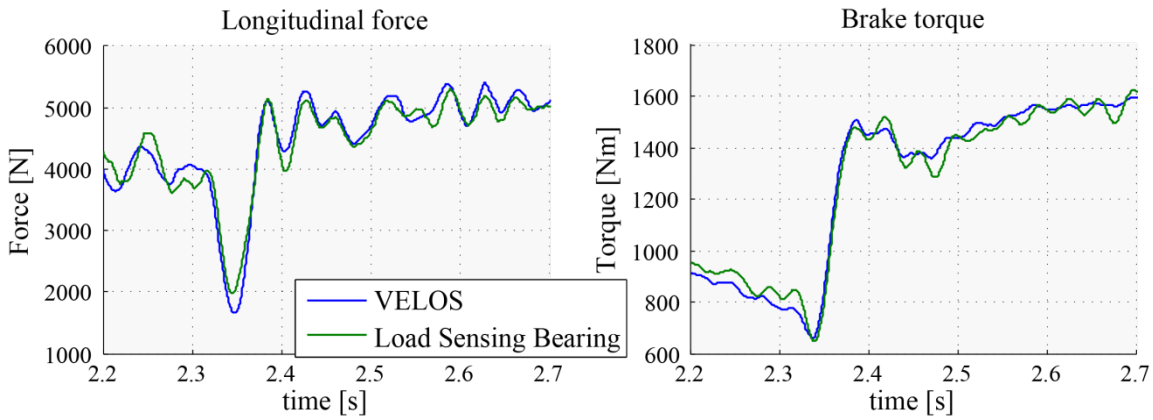

Figure 7: Longitudinal force and brake torque over time

The performance of the applied measurement technique is summarized in Table 1. It is based on 9 experiments which have an average length of 5 seconds. Three of these experiments were used for calibration, whilst the six others are for validation. It can be seen that mean errors are minimal, whilst standard deviations are significant.

	Longitudinal force		Brake torque	
Average load	3948.9 [N]		1147.9 [Nm]	
Mean error	10.5 [N]	0.27%	3.3 [Nm]	0.29%
Standard deviation	278.4[N]	7.05%	60.7[Nm]	5.29%

Table 1: Performance of the load sensing bearing measurement method

Figure 8 shows the power spectral density for estimation of longitudinal force F_x and brake torque T_b using the VELOS measurement rim and load-sensing bearing based on the same set of experiments as used in Table 1. It can be observed that estimation of both longitudinal force and brake torque using the load-sensing bearings is performed precisely for frequencies up to about 10 Hz. For higher frequencies noise in both estimated parameters is increased.

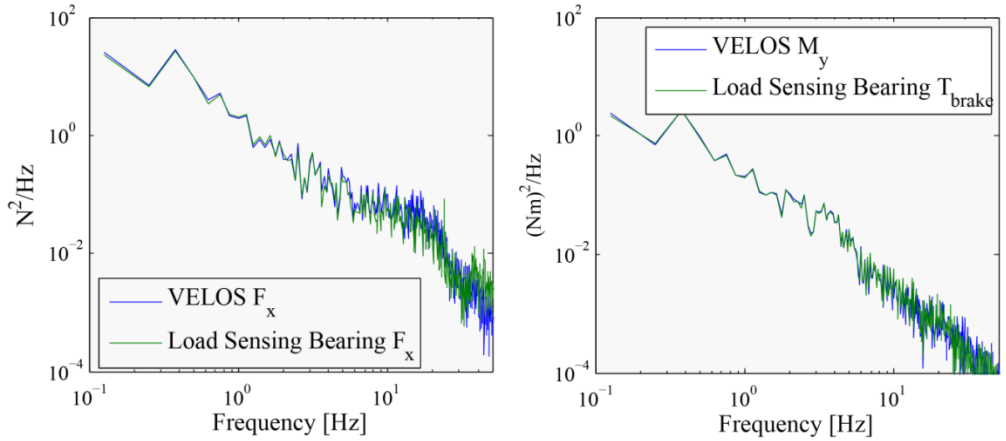

Figure 8: Power spectral densities of VELOS and Load Sensing Bearing load measurements

Improvement of the current performance is expected by further investigations using advanced estimation methods and better measurement/calibration equipment like a Kistler measurement rim.

Anti-lock Braking algorithm

Wheel speed, vehicle speed and brake pressure over time after activation of the load-based algorithm are shown in Figure 9. Five cycles of the algorithm can be observed, which correctly avoid wheel lock from occurring.

Cycling of the algorithm is slightly slower as intended as the brake pressure controller has difficulties performing small pressure increases, which are usually requested in the later stages of phase 2. This problem can be fixed by the improvement of the current approach of brake pressure control.

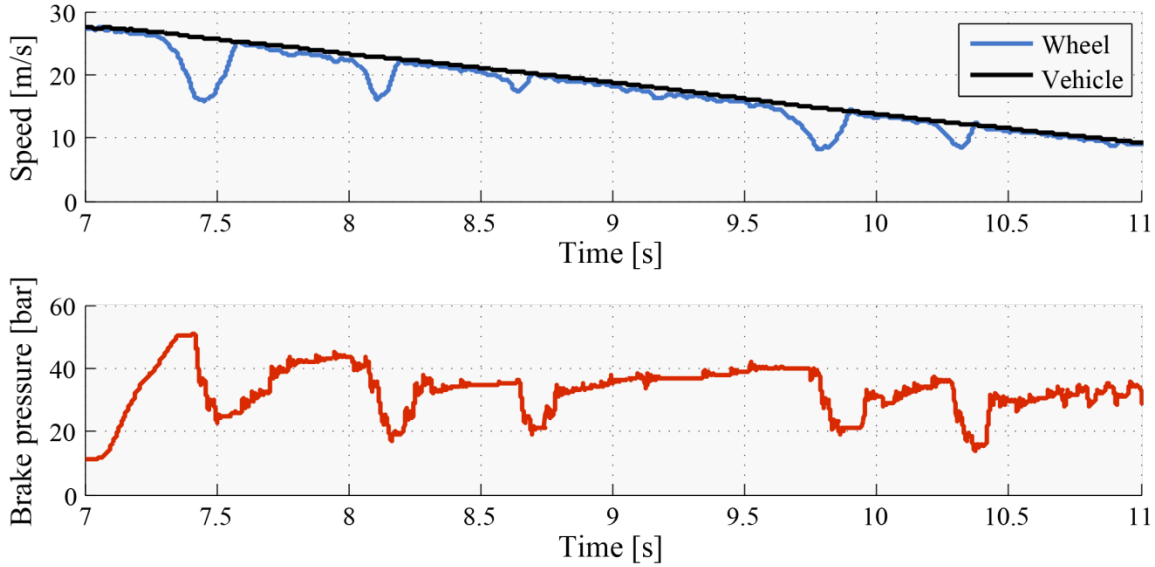

Figure 9: Wheel speed, vehicle speed and brake pressure over time during the load based ABS algorithm

Figure 10 presents the wheel slip (top) and load-based wheel slip derivative control data (bottom) of a single cycle of the proposed ABS algorithm. The difference in brake torque and torque due to the longitudinal force ($T_b - r_w F_x$) is plotted in blue. The boundary conditions of Eqs. 9 and 10 are represented by respectively the black dotted and black solid line. It is clearly visible that wheel slip increases when the torque difference complies to Eq. 10 and slip decreases when Eq. 9 is fulfilled.

Note that measurement errors and noise influence the brake torque difference ($T_b - r_w F_x$) measurement. Therefore, especially when near 0, the sign of the slip derivative might be incorrectly estimated. This can be avoided by proper control settings, i.e. significantly low or high brake torque values.

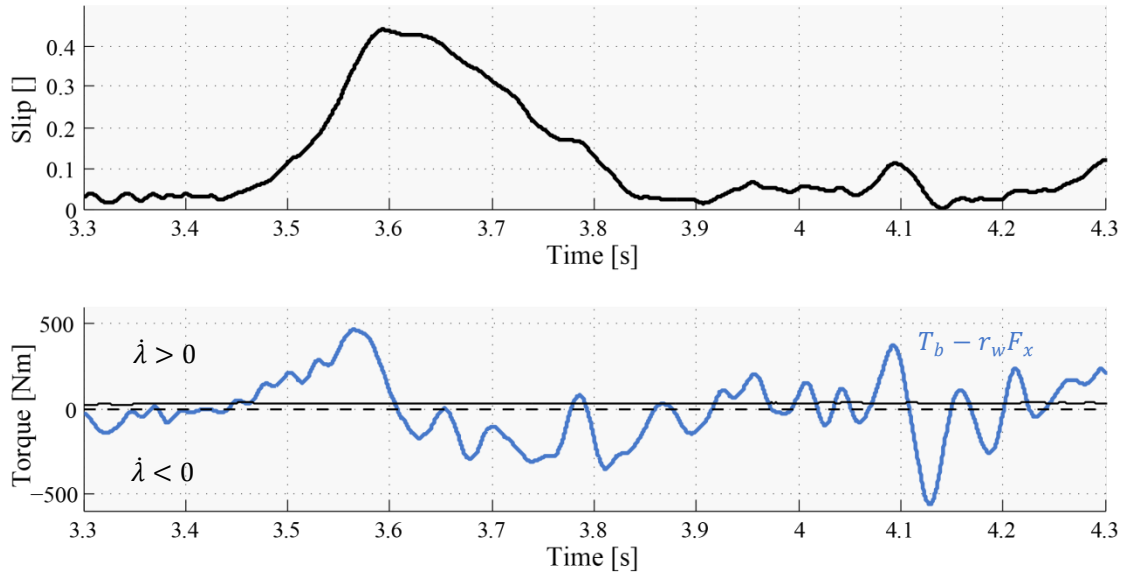

Figure 10: Validation of the load based wheel slip derivative control approach, in which the black dotted and solid line in the lower figure represent the boundary conditions provided in Eqs. 9 and 10

Figure 11 shows the triggering mechanism at work in phase 2 and phase 1 respectively, firing at $t \cong 6.32\ s$ and $t \cong 6.45\ s$. The mechanism triggers a subsequent phase in line with Eq. 16.

The figure also shows that occasionally, as for instance at $6.35 < t < 6.45\ s$, the longitudinal force is significantly influenced by other factors than changes in wheel slip and the subsequent changes of friction. This is probably related to changes in vertical loading due to load transfer, road irregularities or tire un-roundness. The force triggering offset ΔF_{tr} is tuned as discussed in Section IV such that false triggering due to these oscillation is minimal.

Future work will focus on eliminating the normal load dependency of the triggering mechanism by normalization using vertical load F_z. This latter is not implemented yet as the current load-sensing methodology does not provide sufficient bandwidth in the normal load estimation.

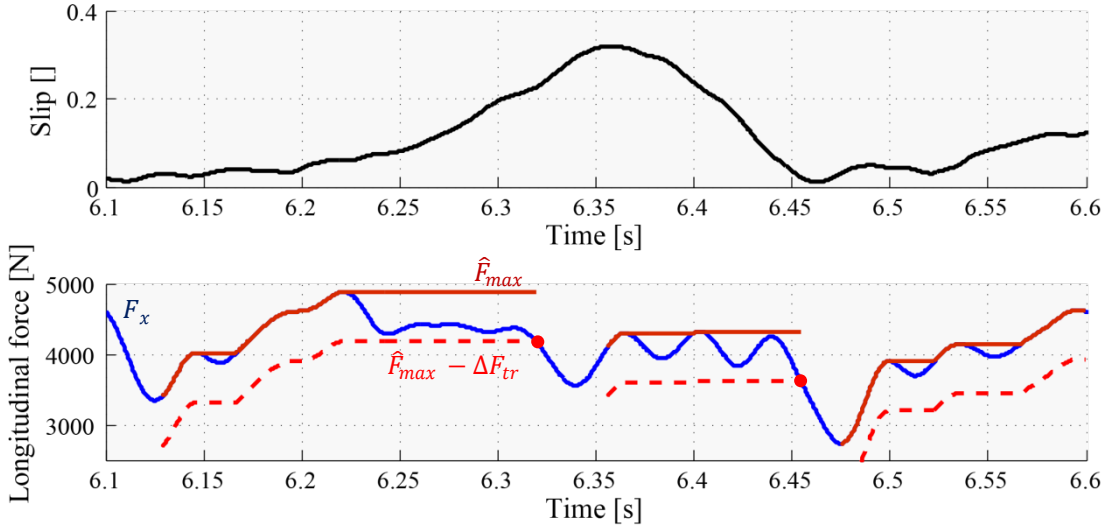

Figure 11: Longitudinal force based triggering mechanism over time

A quantitative analysis of the algorithm performance remains a matter of further investigation as improvements to the brake pressure controller are required for optimal performance.

VIII CONCLUSION AND FUTURE WORK

The paper presents a method to control the wheel slip derivative based on wheel loading. Based on this slip control methodology a novel two phase ABS algorithm with a force based phase switching mechanism is designed. Due to the usage of wheel loads, traditional ABS difficulties like velocity estimation and slip threshold determination and adaptation are circumvented and effects of road friction fluctuations and brake efficiency are minimized. Furthermore a bearing deformation based wheel load measurement methodology is proposed to provide the necessary load measurements. The performance of the load measurement methodology and the proposed ABS algorithm was investigated using an instrumented test vehicle in real road conditions. The results of the presented experimental investigations have demonstrated the feasibility of the proposed methods to control wheel slip for ABS with sufficient accuracy. Meanwhile, the variation of vertical load is still an open issue for the proposed triggering mechanism.

The authors of the paper expect that the current performance of the proposed ABS algorithm can be improved by: (i) more precise control of brake pressure and (ii) a phase trigger mechanism which is invariant of vertical loading. The authors would like to present the updated results in the subsequent publications. In addition, quantitative benchmarking of the proposed and industrial ABS algorithms is planned for the near future.

REFERENCES

[1] *L. Austin and D. Morrey, "Recent advances in antilock braking systems and traction control systems," Proceedings of the Institution of Mechanical Engineers, Part D: Journal of Automobile Engineering, vol. 214, pp. 625-638, 2000.*

[2] *V. Ivanov, D. Savitski, and B. Shyrokau, "A Survey of Traction Control and Anti-lock Braking Systems of Full Electric Vehicles with Individually-Controlled Electric Motors," Vehicular Technology, IEEE Transactions on, vol. PP, pp. 1-1, 2014.*

[3] *M. Corno, M. Gerard, M. Verhaegen, and E. Holweg, "Hybrid ABS Control Using Force Measurement," Control Systems Technology, IEEE Transactions on, vol. 20, pp. 1223-1235, 2012.*

[4] *L. R. Ray, "Nonlinear tire force estimation and road friction identification: simulation and experiments," Automatica, vol. 33, pp. 1819-1833, 1997.*

[5] *M. Suzuki, K. Nakano, A. Miyoshi, A. Katagiri, and M. Kunii, "Method for sensing tire force in three directional components and vehicle control using this method," SAE Technical Paper2007.*

[6] *M. Gobbi, J. Botero, and G. Mastinu, "Global chassis control by sensing forces/moments at the wheels," International Journal of Vehicle Autonomous Systems, vol. 7, pp. 221-242, 2009.*

[7] *F. Cheli, E. Sabbioni, M. Sbrosi, M. Brusarosco, and S. Melzi, "Enhancement of ABS Performance through On-Board Estimation of the Tires' Response by Means of Smart Tires," 2011.*

[8] *H. A. Mol, "Method and sensor arrangement for load measurement on rolling element bearing based on model deformation," ed: Google Patents, 2008.*

[9] *E. de Bruijn, M. Gerard, M. Corno, M. Verhaegen, and E. Holweg, "On the performance increase of wheel deceleration control through force sensing," in Control Applications (CCA), 2010 IEEE International Conference on, 2010, pp. 161-166.*

[10] *D. Capra, E. Galvagno, V. Ondrak, B. Van Leeuwen, and A. Vigliani, "An ABS control logic based on wheel force measurement," Vehicle System Dynamics, vol. 50, pp. 1779-1796, 2012.*

[11] *H. B. Pacejka, Tire and vehicle dynamics vol. 372, 2006.*